Preliminary stable isotope and geochemical investigation of carbonate in the Klondike district

Murray M. Allan[1], James K. Mortensen, and Natalie Cook
Mineral Deposit Research Unit, The University of British Columbia, Vancouver, B.C.

Allan, M.M., Mortensen, J.K., and Cook, N., 2014. Preliminary stable isotope and geochemical investigation of carbonate in the Klondike district. *In:* Yukon Exploration and Geology 2013, K.E. MacFarlane, M.G. Nordling, and P.J. Sack (eds.), Yukon Geological Survey, p. 1-20.

ABSTRACT

Carbonate is an important component of gold-bearing quartz veins in the Klondike district, and also makes up an under-recognized proportion of the Klondike schist host rocks. The predominantly metavolcanic Klondike schist contains carbonate as disseminated porphyroblasts and as coarse quartz-carbonate segregations, and contains rare layers of marble. Chemical staining and LA-ICP-MS analyses reveal that, irrespective of paragenesis, carbonate is dominated by Mg-Fe-Mn calcite. Laser spectroscopic analyses of C and O isotopes reveal that marble is a ^{13}C-enriched isotopic reservoir compared to carbonate in micaceous schist. Carbonate in gold-stage veins has a similar isotopic signature to carbonate in metamorphic segregations and porphyroblasts in the host rocks. We tentatively interpret these results to indicate that the CO_2 component of vein carbonate has been remobilized from local sources during brittle deformation. The results of this study may bear on interpreting the scale of rock-fluid interaction during orogenic gold mineralization in the area.

[1] *mallan@eos.ubc.ca*

INTRODUCTION

The rich placer gold fields of the Yukon's Klondike district are underlain primarily by the Klondike schist – a strongly deformed, Late Permian assemblage of metamorphosed volcanic, volcaniclastic and associated meta-intrusive rocks that make up part of the Yukon-Tanana terrane (Fig. 1). The placer deposits are derived from erosion of orogenic quartz-carbonate-pyrite-gold veins of Late Jurassic age that crosscut the Klondike schist. Auriferous veins in the Klondike formed during regionally widespread brittle-ductile to brittle deformation (D_4 deformation event described by MacKenzie *et al.*, 2008b), an event which is also responsible for the numerous deposits and gold occurrences of the White Gold district (Allan *et al.*, 2013). Several aspects of Klondike vein mineralization have been studied, such as their age (Hunt and Roddick, 1992; Breitsprecher and Mortensen, 2004; J. Mortensen, unpublished data, 2012), fluid conditions and water source (Rushton *et al.*, 1993), structural style (MacKenzie *et al.*, 2008a), and metal sources (Mortensen *et al.*, 2006; J. Mortensen, unpublished data). However, little attention has been paid to the carbonate component of gold-bearing veins in the Klondike. In particular, what is the origin of the carbon, how is it redistributed during hydrothermal and deformation events, and what role may CO_2 play in the transport and precipitation of gold?

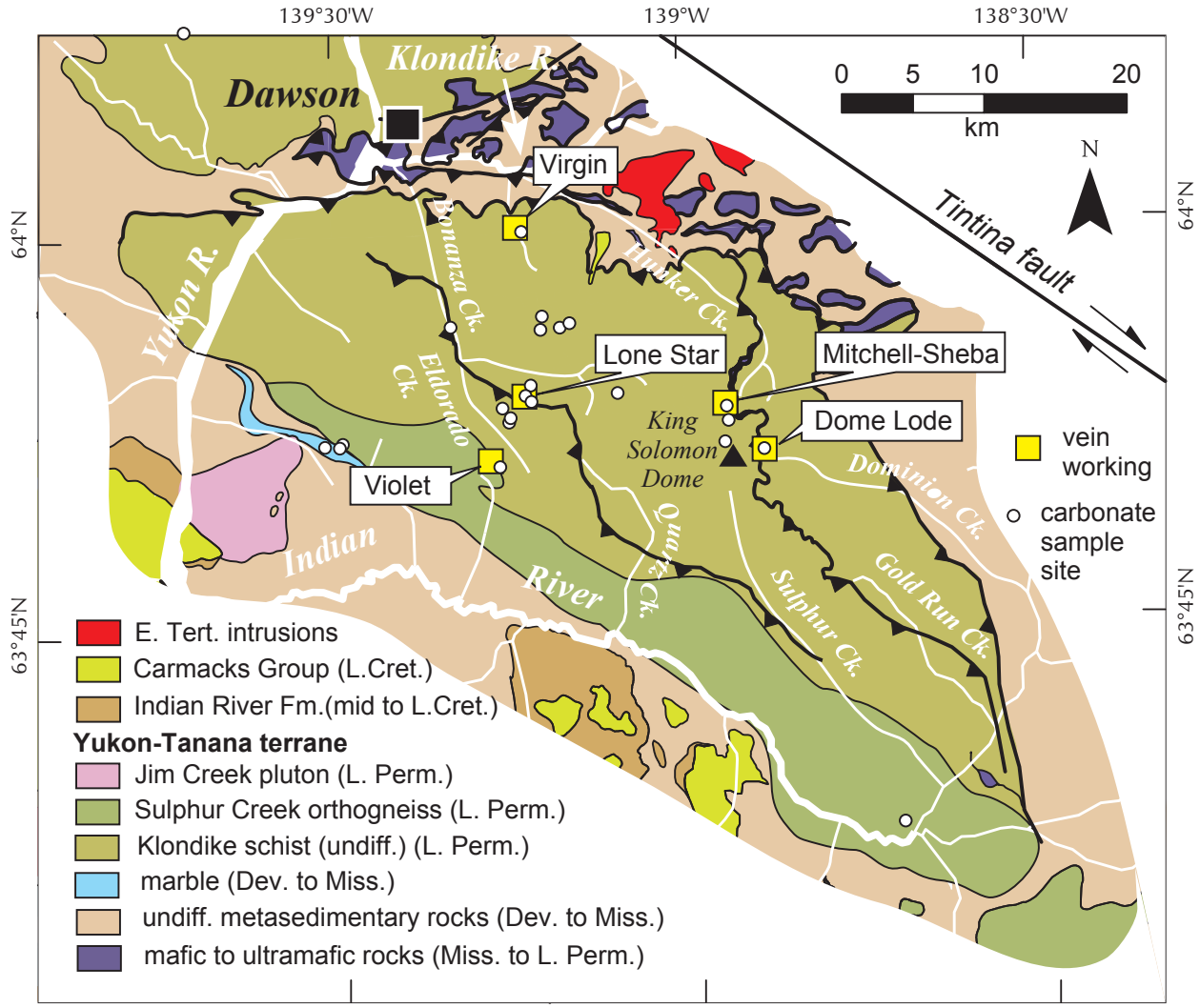

***Figure 1**. Simplified geologic map of the Klondike district, showing the location of carbonate samples and gold-bearing quartz vein workings.*

Carbon dioxide is a ubiquitous component of hydrothermal fluids that form orogenic gold deposits (*e.g.*, Groves *et al.*, 2003). It is recognized directly in fluid inclusions trapped in vein quartz, and is inferred from carbonate alteration haloes in the wallrock of veins. Stable isotopes may be useful in interpreting carbon sources in orogenic gold deposits. Carbon isotopic signatures of fluid inclusions and carbonate minerals in orogenic gold deposits globally range from $\delta^{13}C_{VPDB}$ = -26 to +13 ‰, with distinct modes at $\delta^{13}C_{VPDB}$ = -22 ‰ and -5 ‰ (Beaudoin, 2011) (VPDB = Vienna Pee Dee Belemnite C-isotope standard; VSMOW = Vienna Standard Mean Ocean Water O-isotope standard). More negative $\delta^{13}C$ values are typical of some Phanerozoic deposits hosted in metasedimentary rocks that contain reduced organic carbon (*e.g.*, Kontak and Kerrich, 1997), and more positive values are typical of deposits hosted in volcanic rocks. Although magmatic and mantle sources of carbon have been proposed for some volcanic-hosted orogenic gold systems, the overall distribution of isotopic signatures clearly demonstrates an influence of country rocks on the isotopic geochemistry.

During recent regional investigations of the Late Jurassic gold mineralization in west-central Yukon, we noted that carbonate is an under-recognized component of the Klondike schist. Because carbonate is so efficiently leached in the weathering environment – especially in the presence of acid-generating pyrite – it is commonly not preserved at surface. Instead, it is inferred in surface rock exposures from vuggy cavities or travertine coatings. Regardless, unweathered carbonate is found in many road cuts, trench exposures, and mine workings, and in some localities constitutes a significant rock-forming mineral.

Because carbonate minerals constitute not only a component of gold-bearing quartz veins, but also a locally significant component of the Klondike schist protolith, they provide an opportunity to test whether country rocks are a carbon source during gold mineralization. If so, can variations in isotopic signatures provide insight into the scale of rock-fluid interaction?

In this paper, we present the paragenesis, geochemistry, and carbon and oxygen isotopic signature of carbonate from the Klondike schist, in addition to the stratigraphically and structurally underlying Nasina assemblage. Carbon as graphite was not analyzed in this study, but is an obvious avenue of future work. In the Klondike schist, three modes of carbonate occurrence were sampled and analyzed: (1) "matrix" – carbonate as an essential rock-forming mineral, comprising part of the Late Permian protolith; (2) "segregation" – carbonate concentrated during ductile deformation into foliation-parallel, quartzose segregations; and (3) "vein" – carbonate occurring in late-stage veins that crosscut the dominant metamorphic fabric. The results are discussed in the context of orogenic gold mineralization in the Klondike district.

BACKGROUND

GEOLOGY OF THE KLONDIKE

The Late Permian Klondike assemblage is a thrust-imbricated sequence of metamorphosed arc rocks that underlies most of Klondike gold fields. The Klondike assemblage is composed of metavolcanic rocks of the Klondike schist, and age-equivalent metaplutonic rocks of the Sulphur Creek orthogneiss (Fig. 1). A component of the Klondike schist is quartz ± feldspar augen quartz-feldspar-muscovite ± chlorite ± biotite schist, interpreted as a felsic to intermediate metaporphyry. The Klondike schist ranges in composition from mafic (chloritic schist and minor metagabbro) to felsic (quartz-feldspar-muscovite schist), with rare exposures of impure marble and graphitic schist on the ridge between Eldorado and upper Bonanza creeks (Fig. 1; near the historic Lone Star gold mine, Yukon MINFILE 115O 072). Locally, the Klondike schist is strongly pyritic, and also contains showings of syngenetic, VMS-style galena-chalcopyrite ± gold mineralization (Mortensen, 1990; Mortensen *et al.*, 2006).

The Klondike assemblage is structurally and stratigraphically underlain by variably carbonaceous metasiliciclastic rocks and minor marble of the Devonian to Mississippian Nasina assemblage. These rocks are age-equivalent to volcanic rocks of the Finlayson assemblage, which represent the first phase of arc magmatism in the Yukon-Tanana terrane.

Rocks in the Klondike district have a penetrative metamorphic foliation S_2, which transposes an earlier S_1 fabric. This foliation was developed during the Late Permian Klondike orogeny, when the Yukon-Tanana terrane collided with, and overrode the North American margin (Beranek and Mortensen, 2011). The most common prograde metamorphic assemblage in the Klondike schist is quartz-feldspar-muscovite-chlorite, suggesting greenschist facies peak metamorphic conditions. A superimposed metamorphic fabric, consisting of asymmetric crenulations and a locally pervasive axial planar fabric (S_3), is commonly developed (Fig. 2). This deformation event has been linked to regional thrust faulting in the Early Jurassic (MacKenzie *et al.*, 2008b). A later generation of steep-dipping reverse faults,

angular kink folds, shears, and discordant quartz veins (S_4) is attributed to a subsequent phase of Jurassic deformation (MacKenzie *et al.*, 2008a). Orogenic gold mineralization in the Klondike is closely associated with this deformation phase. Subsequent geologic events include Late Cretaceous to Paleogene magmatism and normal faulting, but these are not relevant to this study.

***Figure 2**. Sample of Klondike schist, showing an F_3 fold with an accumulation of quartz and calcite in the hinge zone. Clots of partially leached calcite are indicated by the white arrows. Quartz and calcite are interpreted to have migrated into low-strain fold hinges during D_3 deformation, potentially from pre-existing, D_2-generation segregations.*

CARBONATE OCCURRENCES IN THE KLONDIKE

Nasina assemblage: A belt of marble is exposed as road rubble north of the mouth of the Indian River (Fig. 1). Rocks in this area include calcite marble as well as calcite and graphite-bearing quartz-muscovite schist and tremolite schist. Discordant calcite veins cutting the metamorphic foliation are common.

Klondike schist: Where preserved, carbonate in Klondike schist occurs as tan to orange-weathering clots in coarse-grained segregations along the S_1/S_2 metamorphic foliation (Fig. 3). Where carbonate is leached, the rocks contain vuggy cavities lined with a fine black, manganiferous coating. The coarsest accumulations of carbonate occur in the hinges of F_3 folds (Fig. 2), suggesting that quartz and carbonate were mobilized by dynamic recrystallization during ductile deformation. More rarely, carbonate occurs as 1 to 5-mm porphyroblasts in the silicate matrix. The metaporphyry member of the Klondike schist, well exposed in a reclaimed trench near the Violet gold mine (Yukon MINFILE 115O 073; Fig. 1), contains rare, pink, coarse-grained carbonate in foliation-parallel, quartz-rich segregations (Fig. 3C-D).

Klondike schist - marble: Blocks of tan-weathering marble are observed east of the Lone Star gold mine (Figs. 1 and 4), in a reclaimed trench near the 7 Pup of Victoria Gulch. Muscovite and quartz together comprise 20 to 60 % of the rock volume. Foliation-parallel, coarse carbonate-quartz segregations are observed.

D_4-Stage Veins: Carbonate-bearing veins are commonplace in steep, D_4 deformation zones in the Klondike schist, and more rarely in the Sulphur Creek orthogneiss and Nasina assemblage metasediments. In all cases, veins are discordant to the penetrative metamorphic schistosity. Carbonate is a common component of quartz veins, occurring either on the selvages or interiors of veins as a primary hydrothermal mineral (Fig. 5), or in the immediately surrounding wallrock as an alteration phase. Only hydrothermal carbonate from vein material was sampled in this study. Vein carbonate is typically blocky in quartz-carbonate veins, and blocky to fibrous in carbonate-only veins. Where preserved, carbonate is creamy white to brown to orange-weathering.

METHODS

SAMPLING

Carbonate-bearing samples were collected from outcrop, subcrop, historic exploration and mine workings, and drill core. The samples contained carbonate either as a component of the rock matrix, within coarse-grained, quartz-rich segregations parallel to the metamorphic foliation, or in crosscutting veins. Rock samples that had coatings of travertine, iron/manganese oxides, or lichen were sandblasted to expose fresh surfaces without removing excessive amounts of carbonate. Sample locations and lithology are listed in Table 1.

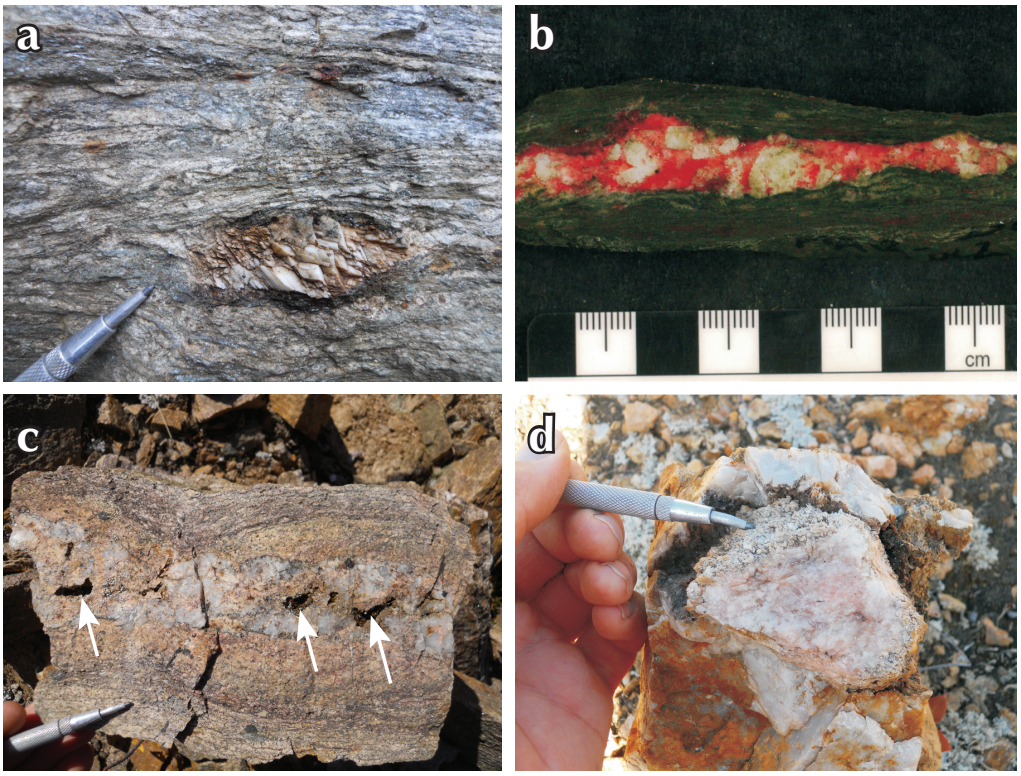

Figure 3. *Examples of carbonate-bearing segregations in Klondike schist: (a) lensoid calcite segregation in quartz-feldspar-muscovite-chlorite schist (Dome Lode; Yukon MINFILE 115O 067); (b) chloritic schist with a coarse quartz-calcite segregation, calcite stained by alizarin red S (Dome Lode); (c) boudinaged quartz-carbonate segregation in feldspathic metaporphyry (Violet); and (d) coarse clot of pink calcite within a quartz segregation (Violet).*

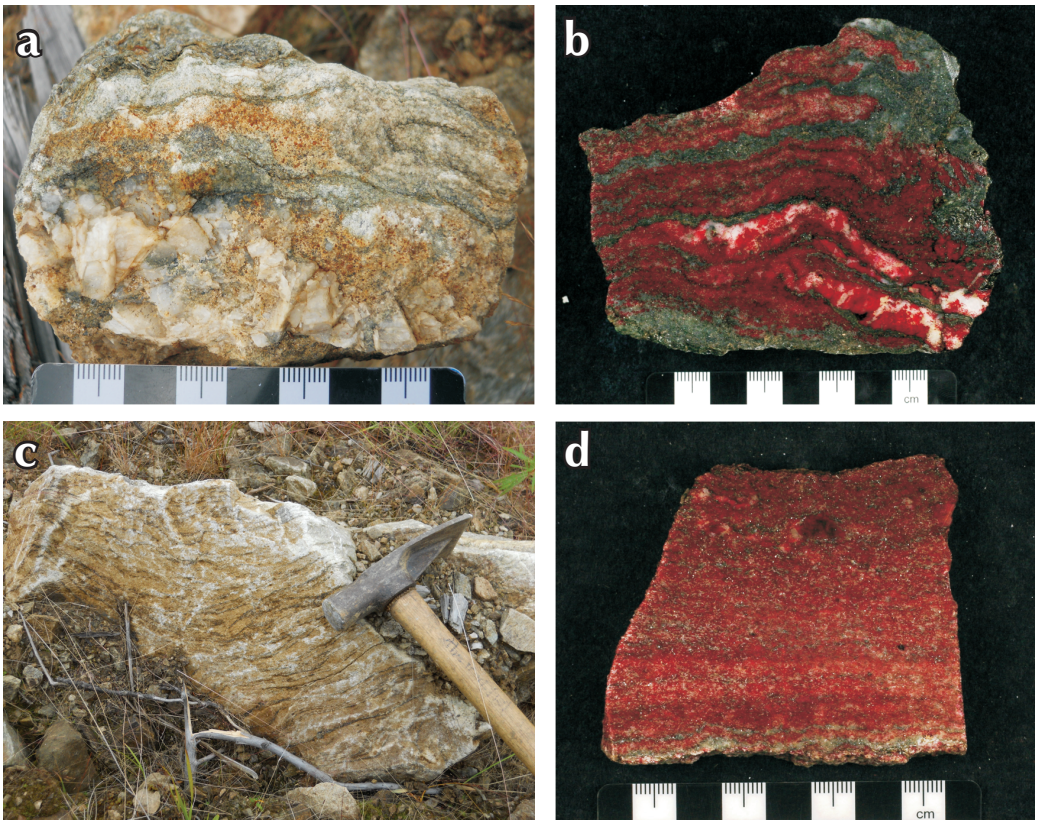

Figure 4. *Rare examples of marble from the Klondike assemblage: (a) folded quartz-muscovite-calcite schist with coarse quartz-calcite segregation; (b) same sample as in (a), calcite stained with alizarin red S; (c) sample of banded marble, with quartz and muscovite as the main impurities; and (d) same sample as in (c), calcite stained with alizarin red S.*

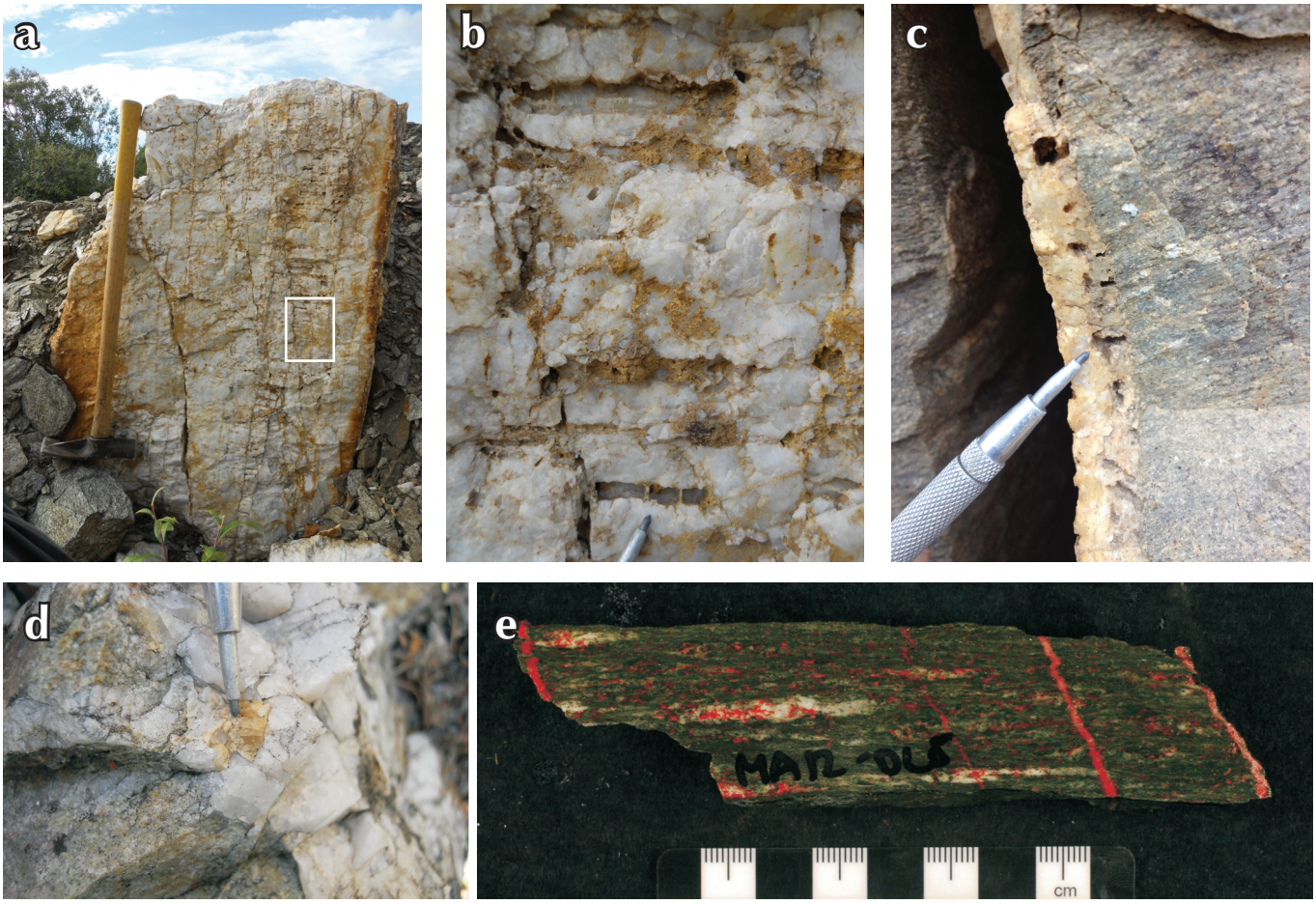

***Figure 5**. Examples of carbonate-bearing veins from the Klondike district: (a-b) milky quartz-carbonate vein of the Mitchell-Sheba vein system (Yukon MINFILE 115O 068). Carbonate is strongly leached; inset (b) shows columnar growth of quartz and carbonate (inferred from leached pits) perpendicular to the vein margins; (c) quartz vein with leached pits after blocky calcite. The vein is hosted by Sulphur Creek orthogneiss; (d) coarse calcite at the margin of a quartz vein (Virgin; Yukon MINFILE 116B 007); and (e) sample of Klondike schist with three modes of calcite occurrence: disseminated grains, quartz-calcite segregations, and discordant veins (Dome Lode).*

STAINING

Cut rock slabs and the curved, outer surfaces of halved drill core samples were treated with a sequential carbonate staining technique (modified from Hitzman, 1999) to determine the carbonate minerals present. Samples were pre-etched in 5% HCl v/v for 30 to 60 s, depending on how vigorously the carbonate reacted, and rinsed in water. A calcite-sensitive staining solution was prepared by dissolving 2.0 g of alizarin red S (sodium 3,4-dihydroxy-9,10-dioxo-2-anthracene sulphonate) in 250 mL of 2% v/v HCl. A second solution, sensitive to ferrous iron in carbonate, was prepared by dissolving 2.0 g of potassium ferricyanide ($K_3Fe^{III}(CN)_6$) in 250 mL of 2% HCl v/v. Samples were soaked in a 5-mm deep basin of alizarin red S solution for 30 s, rinsed in water, blotted dry, and photographed. Samples that stained bright red were interpreted to contain nearly pure calcite, whereas samples that stained wine red, red-brown, or purple were interpreted to contain impure calcite. Samples that were either unreactive with alizarin red S or stained very pale pink were interpreted to be dolomite. Samples were then stained in the potassium ferricyanide solution for 60 s, rinsed, blotted, and photographed. Carbonate samples that reacted to produce a blue, indigo, or purple stain were interpreted to contain ferrous iron.

MICROSAMPLING

Carbonate microsampling was required for two analytical procedures: (1) carbon and oxygen isotopic analysis by laser spectroscopy; and (2) compositional analysis by laser ablation – inductively coupled plasma mass spectrometry (LA-ICP-MS).

***Table 1**. Sample descriptions.*

Sample	Area	Sample Type	Location (NAD83/ UTM Zone 7N)		Rock Name	Group	Carbonate Type		
			Easting (m)	Northing (m)			Matrix	Seg'n	Vein
KLONDIKE ASSEMBLAGE SAMPLES									
05-LS-25_73.4m	Lone Star Ridge	drill core	586849	7086318	qtz-fs-ms schist	felsic	fcc	fcc*	
05-LS-25_75.0m	Lone Star Ridge	drill core	586849	7086318	qtz-fs-ms schist	felsic	fcc	fcc (2)	
06-LS-19_68.0m	Lone Star Ridge	drill core	586595	7086500	qtz augen schist	metaporphyry	(1)		
06-NZ-01_65.7m	Oro Grande Gulch / Eldorado Creek	drill core	584955	7085697	qtz augen schist	metaporphyry	fcc* (1)		
06-NZ-01_65.8m	Oro Grande Gulch / Eldorado Creek	drill core	584955	7085697	qtz augen schist	metaporphyry		fcc (1)	
BU-07-02_108.3m	Gay Gulch / Eldorado Creek	drill core	585473	7084751	qtz-fs-ms-chl schist	felsic			fcc* (1)
BU-07-02_114.6m	Gay Gulch / Eldorado Creek	drill core	585473	7084751	qtz-fs-ms-chl schist	felsic			fcc* (1)
BU-07-02_146.2m	Gay Gulch / Eldorado Creek	drill core	585473	7084751	qtz-fs-ms-chl schist	felsic	fcc		fcc (1)
BU-07-03_64.0m	Gay Gulch / Eldorado Creek	drill core	585539	7084949	qtz-fs-ms schist	felsic			fcc* (1)
BU-07-03_78.6m	Gay Gulch / Eldorado Creek	drill core	585539	7084949	qtz-fs-ms schist	felsic			fcc* (1)
BU-07-03_83.1m	Gay Gulch / Eldorado Creek	drill core	585539	7084949	qtz augen schist	metaporphyry			fcc* (1)
BU-07-03_91.7m	Gay Gulch / Eldorado Creek	drill core	585539	7084949	qtz-fs-ms schist	felsic			fcc* (1)
BU-07-04_100.5m	Gay Gulch / Eldorado Creek	drill core	585557	7085000	qtz-fs-ms schist	felsic			fcc* (1)
DDH-04-03_283.0m	Upper Bonanza / Last Chance Ridge	drill core	589201	7091349	qtz-fs-ms schist	felsic			fcc* (1)
DDH-04-04_106.5m	Upper Bonanza / Last Chance Ridge	drill core	589799	7091698	qtz-fs-ms schist	felsic			fcc (1)
DDH-04-04_108.5m	Upper Bonanza / Last Chance Ridge	drill core	589799	7091698	qtz-fs-ms schist	felsic	fcc		fcc (1)
DDH-04-04_135.8m	Upper Bonanza / Last Chance Ridge	drill core	589799	7091698	qtz-fs-ms schist	felsic			cc* (1)
DDH-04-04_87.0m	Upper Bonanza / Last Chance Ridge	drill core	589799	7091698	qtz augen schist	metaporphyry			fcc* (1)
DDH-04-05_149.3m	Upper Bonanza / Last Chance Ridge	drill core	587776	7091264	qtz augen schist	metaporphyry			fcc* (1)
DDH-04-05_265.0m	Upper Bonanza / Last Chance Ridge	drill core	587776	7091264	qtz augen schist	metaporphyry			fcc* (1)
DDH-04-05_314.5m	Upper Bonanza / Last Chance Ridge	drill core	587776	7091264	qtz augen schist	metaporphyry			fcc* (2)
DDH-04-05_320.5m	Upper Bonanza / Last Chance Ridge	drill core	587776	7091264	qtz augen schist	metaporphyry			fcc* (1)
DDH-04-05_322m	Upper Bonanza / Last Chance Ridge	drill core	587776	7091264	qtz augen schist	metaporphyry			fcc* (1)
DDH-04-05_332.4m	Upper Bonanza / Last Chance Ridge	drill core	587776	7091264	qtz augen schist	metaporphyry			fcc* (2)
DDH-04-05_333.6m	Upper Bonanza / Last Chance Ridge	drill core	587776	7091264	qtz augen schist	metaporphyry	fcc		fcc* (1)
DDH-04-06_281.3m	Upper Bonanza / Last Chance Ridge	drill core	587778	7092124	qtz augen schist	metaporphyry			fcc* (1)
DDH-04-06_32.0m	Upper Bonanza / Last Chance Ridge	drill core	587778	7092124	qtz augen schist	metaporphyry			fcc (1)
K70	7 Pup / Victoria Gulch	trench	587020	7087280	ms marble	marble	fcc (1)		
K71	7 Pup / Victoria Gulch	trench	587023	7087287	ms marble	marble	fcc* (1)		
K72	7 Pup / Victoria Gulch	trench	587026	7087297	ms mable	marble	fcc (2)		
MA12-DL1	Hunker Dome (Dome Lode)	trench	602646	7084060	qtz-fs-ms schist	felsic		* (3)	
MA12-DL2	Hunker Dome (Dome Lode)	trench	602646	7084060	qtz-fs-ms schist	felsic		fcc (1)	
MA12-DL3	Hunker Dome (Dome Lode)	trench	602646	7084060	qtz-fs-ms schist	felsic		* (2)	
MA12-DL4	Hunker Dome (Dome Lode)	trench	602646	7084060	qtz-fs-ms schist	felsic		cc (2)	
MA12-DL5	Hunker Dome (Dome Lode)	trench	602646	7084060	qtz-fs-ms schist	felsic			* (1)
MA12-DL6	Hunker Dome (Dome Lode)	trench	602646	7084060	chl schist	mafic	fcc (1)	fcc* (1)	fcc* (2)
MA12-DL7	Hunker Dome (Dome Lode)	trench	602646	7084060	chl schist	mafic		fcc* (1)	fcc* (1)
MA12-DL8	Hunker Dome (Dome Lode)	trench	602646	7084060	chl schist	mafic	cc (2)	fcc	fcc* (1)
MA12-DL9	Hunker Dome (Dome Lode)	trench	602646	7084060	chl schist	mafic			* (2)
MA12-K03	Top of the World Hwy.	outcrop	562595	7112051	qtz-fs-ms schist	felsic	fcc/cc*		cc
MA12-K05	Top of the World Hwy.	outcrop	562595	7112051	chl-tlc schist	mafic		cc* (2)	

***Table 1**. continued.*

Sample	Area	Sample Type	Location (NAD83/ UTM Zone 7N)		Rock Name	Group	Carbonate Type		
			Easting (m)	Northing (m)			Matrix	Seg'n	Vein
MA12-K07	7 Pup / Victoria Gulch	float	586913	7087144	ms marble	marble	fcc* (4)		
MA12-K08	7 Pup / Victoria Gulch	float	586913	7087144	ms marble	marble	fcc* (2)		
MA12-K09	7 Pup / Victoria Gulch	float	586913	7087144	ms marble	marble	fcc* (2)	fcc* (1)	
MA12-K10	7 Pup / Victoria Gulch	float	586913	7087144	ms marble	marble	fcc* (3)		
MA12-K11	7 Pup / Victoria Gulch	float	586913	7087144	ms marble	marble	fcc (1)		
MA12-K12	7 Pup / Victoria Gulch	float	586913	7087144	ms marble	marble	fcc* (2)		
MA12-K14	Bonanza Creek (near Magnet Gulch)	outcrop	581393	7091468	chl schist	mafic		fcc (2)	
MA12-K16	Upper Bonanza road	outcrop	593129	7086755	chl schist	mafic		fcc (1)	
MA12-K17	King Solomon Dome	outcrop	600775	7083353	chl schist	mafic	fcc* (2)		
MA12-K19	Scriber Creek (mouth)	outcrop	613377	7056823	qtz-fs-ms schist	felsic			(1)
MA12-K20	Hunker Dome (Mitchell)	trench	600790	7085848	chl schist	mafic	fcc* (2)		fcc (1)
MA12-K21	Hunker Dome (Mitchell)	trench	600790	7085848	chl schist	mafic	fcc* (1)		fcc (1)
MA12-SH1	Hunker Dome (Sheba)	outcrop	601000	7085000	chl schist	mafic		fcc* (4)	
MA12-SH2	Hunker Dome (Sheba)	outcrop	601000	7085000	chl schist	mafic		fcc* (3)	
MA12-SH3	Hunker Dome (Sheba)	outcrop	601000	7085000	chl schist	mafic	fcc (1)		fcc* (1)
MA12-VG1	Bear Creek (Virgin)	mine dump	586282	7098104	qtz augen schist	metaporphyry			* (1)
MA12-VG2	Bear Creek (Virgin)	mine dump	586282	7098104	qtz augen schist	metaporphyry			* (1)
MA12-VG3	Bear Creek (Virgin)	mine dump	586282	7098104	qtz augen schist	metaporphyry			* (1)
MA12-VG4	Bear Creek (Virgin)	mine dump	586282	7098104	qtz augen schist	metaporphyry			* (1)
MA12-VG5	Bear Creek (Virgin)	mine dump	586282	7098104	qtz augen schist	metaporphyry			* (1)
MA12-VG6	Bear Creek (Virgin)	mine dump	586282	7098104	qtz augen schist	metaporphyry			* (1)
MA12-VL5	Violet Ridge	trench float	584905	7081545	qtz-fs-bt schist	metaporphyry			* (2)
MA12-VL6	Violet Ridge	trench float	584905	7081545	qtz-fs-bt schist	metaporphyry		(3)	
MA12-VL7	Violet Ridge	trench float	584905	7081545	qtz-fs-bt schist	metaporphyry			fcc* (2)
MA12-VL8	Violet Ridge	trench float	584905	7081545	qtz-fs-bt schist	metaporphyry			* (2)
NASINA ASSEMBLAGE SAMPLES									
MA12-NAS5	near Jim Creek pluton	float	573633	7083041	cc-grph schist	calcareous schist	fcc (1)		
MA12-NAS6	near Jim Creek pluton	float	573633	7083041	cc-grph schist	calcareous schist	* (1)		* (3)
MA12-NAS7	near Jim Creek pluton	float	573633	7083041	grph-trem schist	calcareous schist	fcc (3)		
MA12-NAS8	near Jim Creek pluton	float	573633	7083041	cc-grph schist	calcareous schist		* (1)	
MA12-NAS9	near Jim Creek pluton	float	572526	7082873	cc marble	marble	fcc* (2)		
MA12-NAS10	near Jim Creek pluton	float	572526	7082873	cc marble	marble	fcc* (4)		
MA12-NAS11	near Jim Creek pluton	float	573562	7082892	cc marble	marble	* (1)		
MA12-NAS12	near Jim Creek pluton	float	573577	7082904	cc marble	marble	* (2)		

NOTES

qtz= quartz; ms = muscovite; fs = feldspar; chl = chlorite; bt = biotite; cc = calcite; grph = graphite; trem = tremolite

Under the heading "Carbonate Type":

cc = calcite (interpreted from staining)

fcc = ferroan calcite (interpreted from staining)

* = carbonate analyzed by LA-ICP-MS

(#) = number of C and O isotopic analyses

Samples of paragenetically distinct carbonate were removed from rock samples with a Dremel® rotary tool equipped with a tungsten carbide bit. Approximately 35 to 100 mg of powdered carbonate was collected on weigh paper and transferred to glass vials. Where silicate minerals could not be avoided during microsampling, sample sizes were scaled up accordingly. The tungsten carbide bit was cleaned in 10% HCl v/v followed by ethanol between samples. For some uncut samples, a clean stainless steel mortar and pestle were used to crush coarse fragments of carbonate to a powder.

For compositional analysis by LA-ICP-MS, single carbonate fragments between 1 and 4 mm were selected. For each paragenetic occurrence or composition of carbonate identified, a single grain was carefully sampled using a stainless steel point and placed in a grid on double-sided tape. Samples were mounted in epoxy, ground on 400 and 600 grit sandpaper, and polished sequentially using 6µm, 3µm, and 1 µm diamond, each for 4 minutes with 6 lb pressure.

CHEMICAL ANALYSIS BY LA-ICP-MS

Epoxy-mounted carbonate grains were analyzed at The Pacific Centre for Isotopic and Geochemical Research of UBC using a Resonetics® RESOlution M-50-LR 193-nm ArF excimer laser system, coupled to an Agilent 7700x quadrupole ICP-MS. Samples were ablated in the presence of helium carrier gas, which was delivered to the ICP-MS via polytetrafluoroethylene tubing equipped with a "squid" dispersion device to smooth out the resulting ICP-MS signal. Each carbonate grain was ablated five to ten times with a 24 µm diameter laser spot, pulsed at 10 Hz and having 100 mJ of energy. Each spot was ablated for 40 seconds, followed by 40 seconds of instrument flush time. The analytical sequence consisted of up to 60 spot analyses, and was bracketed by two analyses each of NIST 610 and 612 glass external standards. The NIST 610 and 612 external standards were also inserted between every 10 and 20 spot analyses, respectively. The isotopes analyzed were (dwell times in milliseconds): ^{23}Na (15), ^{25}Mg (100), ^{27}Al (15), ^{29}Si (15), ^{39}K (100), ^{43}Ca (40), ^{55}Mn (30), ^{57}Fe (30), ^{66}Zn (100), ^{88}Sr (30), ^{89}Y (100), ^{137}Ba (30), ^{139}La (30), ^{143}Nd (100), ^{208}Pb (30), and ^{238}U (30). Aluminum, silicon, potassium, and sodium were primarily analyzed as tracers of silicate contaminant material.

Time-resolved ICP-MS signals were background-corrected and converted from count ratios into mass ratios using background-corrected signals from the NIST 610 and NIST 612 external standards. Background corrections, signal integrations, drift corrections, and concentration calculations were carried out with the Matlab®-based computer program SILLS (Allan *et al.*, 2010), which allows individual portions of time-resolved signals to be selected. For each 40-second carbonate signal, the first 1-2 seconds of signal was discarded due to possible surface contamination, and the final 20 seconds was rejected due to possible element fractionation at greater ablation depths. Signals for ^{29}Si and/or ^{27}Al, ^{39}K, or ^{23}Na signals were interpreted as silicate contamination, in which case either the analysis was rejected or the carbonate-only portion of the time-series signal was integrated.

The major to trace element composition of each carbonate sample is expressed as the average of all spot analyses. Errors in element concentration are expressed as the standard deviation of the five to ten separate determinations, which significantly exceeds the analytical error associated with an individual measurement. The most significant cations (Ca, Mg, Fe, and Mn) are expressed as a molar ratio of the total cations. Trace element concentrations are expressed in µg/g on the basis of the molar weight of (Ca, Fe, Mg, Mn)CO_3, which is individually determined for each sample.

C AND O ISOTOPIC ANALYSIS BY LASER SPECTROSCOPY

Powdered carbonate samples were analyzed for $^{13}C/^{12}C$ and $^{18}O/^{16}O$ ratios, using off-axis integrated cavity output spectroscopy (OA-ICOS), closely following the technique of Barker *et al.* (2011). Between 35 and 100 mg of powdered carbonate was weighed and put into a clean borosilicate glass test tube and sealed with a butyl rubber septum. Between 0.2 and 0.3 mL of 85 % H_3PO_4 was injected into the sample tube, the tube was placed in an aluminum heating block, and left to react with the carbonate sample for 1 h at 72 °C. Prior to introducing the carbon dioxide reaction product to the analyzer, the OA-ICOS instrument (Los Gatos Research, model 908-0021) was flushed with dry laboratory air, and pumped down to pressure below 0.5 kPa. The carbon dioxide analyte, up to this point contained within a sealed test tube, was passed via tubing through a glass cold trap contained within a -78 °C bath of dry ice and ethanol to remove any water vapor. The dry CO_2 sample was then introduced via stainless steel tubing into to the OA-ICOS instrument, where carbon and oxygen isotope ratios of the CO_2 were recorded from the absorption spectra of isotopologues $^{12}C^{16}O^{18}O$, $^{13}C^{16}O^{16}O$, and $^{12}C^{16}O^{18}O$ in the near-infrared wavelength region.

Samples that generated sulphurous gas in the isotope analyzer revealed contamination by pyrite at the microdrilling stage, and were rejected due to spectral interferences. Samples contaminated by silicate material (*e.g.*, quartz or muscovite) are unaffected because only the carbonate component reacts with phosphoric acid.

In-house calcite standard BN13 ($\delta^{13}C_{VPDB}$ = 1.84‰; $\delta^{18}O_{VSMOW}$ = 13.64‰) was inserted into the analytical sequence every five unknowns to calculate errors and assess instrument drift. Analytical reproducibility ranged from 0.2 to 1.8 ‰ for $\delta^{13}C$ (±1σ) and 0.5 to 1.0‰ for $\delta^{18}O$ (±1σ). Higher than expected $\delta^{13}C$ errors for some samples were attributed to unusually warm lab conditions.

Sample duplicates, obtained by microdrilling the same geologic feature twice, were inserted every twentieth sample, and showed good correlations. Analytical duplicates, obtained by splitting the carbonate powder into two aliquots, were run every fifth sample, and show excellent correlations. The instrument was calibrated prior to analysis using calcite standards of known isotopic composition (Barker *et al.*, 2011).

RESULTS

CARBONATE CHEMISTRY

The alizarin red S and potassium ferricyanide staining indicated that the vast majority of carbonate, regardless of host rock lithology or mode of carbonate occurrence, is Fe-bearing calcite. In a small number of cases, samples produced only a very weak pink stain with alizarin red S, and the potassium ferricyanide produced a bright blue stain; in these cases, ferroan dolomite or ankerite was interpreted to be present. No distinguishing feature (*e.g.*, rock type) appears to control where ferroan dolomite is likely to occur. A small number of samples reacted only to alizarin red S, indicating a nearly pure calcite composition. These compositions are more typical of marble and calcareous schist of the Nasina assemblage.

Within a given sample, the colour and intensity of stain was generally consistent. This observation indicates little compositional zoning, and supports the approach of analyzing small representative grains by LA-ICP-MS.

The LA-ICP-MS results are reported in Appendix 1. Of 63 samples analyzed, 54 are "impure" calcite, containing subequal molar quantities of Mg, Fe, and Mn. In these samples, auxiliary cations comprise 0.7 to 6.4% of the cation inventory on a molar basis. In these samples, the other elements analyzed by LA-ICP-MS are in significantly lower abundance (median concentrations shown in parentheses): Sr (1001 µg/g); Y (22.3 µg/g); Ba (13.1 µg/g); Pb (9.6 µg/g); Nd (3.4 µg/g); Zn (3.0 µg/g); La (1.2 µg/g); and U (0.02 µg/g). Concentrations of these elements are similar in Mg-Fe-Mn calcite and ferroan dolomite samples, although the latter contains one to two orders of magnitude more Zn.

The concentrations of Mg and Fe show a good correlation, whereas the correlation of Mn to these elements is weaker. Sr and Y also show a reasonable correlation. A close correlation between La and Nd is observed over four orders of magnitude concentration variation (Fig. 6).

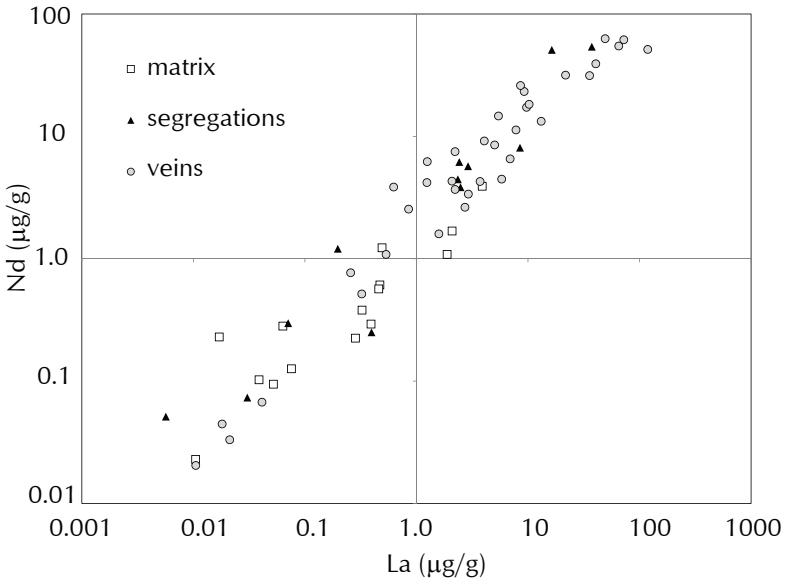

Figure 6. *La vs. Nd concentrations in Klondike schist carbonate samples. Data are divided into matrix (porphyroblasts), segregations, and veins. Data points represent the average La and Nd concentration of several point LA-ICP-MS spot analyses per sample. Errors bars are omitted for clarity.*

CARBON AND OXYGEN ISOTOPES

Carbon and oxygen isotope determinations for Klondike carbonate samples are presented in Appendix 2. Figure 7A shows the dataset coded by lithologic subunits, which include the felsic, mafic, metaporphyritic, and marble variants of the Klondike schist, as well as calcareous schist and marble variants of the Nasina assemblage.

Calcite marble of the Nasina assemblage forms a distinct data cluster with $\delta^{13}C_{VPDB}$ values of -2 to 4‰ and $\delta^{18}O_{VSMOW}$ values of +11 to +17‰. Relative to the Nasina marble, the calcareous, graphitic schist of the Nasina assemblage is shifted to lower $\delta^{13}C_{VPDB}$ (-10 to -6‰) and has similar, but more variable $\delta^{18}O_{VSMOW}$ values (+9 to +21‰).

The Klondike schist samples form two main isotopic populations. The Mg-Fe-Mn calcite marble samples cluster around $\delta^{13}C_{VPDB}$ = +1 to +5‰ and $\delta^{18}O_{VSMOW}$ = +5 to +10‰, which is ^{18}O-depleted by ~5 ‰ relative to the Nasina marble samples. In contrast, the remaining Klondike schist carbonate samples plot at much lower $\delta^{13}C_{VPDB}$ values (generally between -13 and -4‰), and over a much wider range of $\delta^{18}O_{VSMOW}$ values (-8 to +15‰). The range in C and O isotopic compositions between the mafic, felsic, and metaporphyry subunits of the Klondike schist overlap, with the exception of a few anomalously positive $\delta^{13}C_{VPDB}$ values in the mafic schist.

The extreme outlier at $\delta^{13}C_{VPDB}$ = -36‰ in Figure 7 is a sample of pink calcite in a quartz-rich segregation within quartz augen schist near the Violet gold occurrence (Fig. 4D). The sample had a chalky alteration rind which was avoided during microdrilling, but the interior of the sample was neither visibly altered nor unusual in chemical composition. Furthermore, the sample was microdrilled and analyzed in triplicate to rule out random sampling or analytical error. The Klondike assemblage's stratigraphy is dominated by meta-igneous rocks, so influence from a ^{13}C-depleted, organically-derived local carbon source is unlikely. Intrusive units of the Klondike assemblage are typically oxidized, so carbonate is unlikely to have inherited its extremely light $\delta^{13}C$ signature from intrusion-related CH_4. Our preferred explanation is that such low $\delta^{13}C_{VPDB}$ values are the result of extreme open-system Rayleigh fractionation behaviour during metamorphism.

Figure 7B discriminates between carbonate occurring as rock matrix, in segregations, and in veins. The isotopic composition of carbonate in segregations and veins strongly overlap (most hosted in Klondike schist). The significance of this observation is discussed in the following section.

DISCUSSION

Five important points emerge from this study:

1. Origin of Marble: Marble of the Klondike schist and Nasina assemblage is isotopically distinct from the silicate Klondike schist samples, with slightly positive $\delta^{13}C_{VPDB}$ values (+1 to +5‰) and a much narrower range of $\delta^{18}O_{VSMOW}$ values (+5 to +10‰). The $\delta^{13}C_{VPDB}$ isotopic signatures of both Klondike and Nasina marble are consistent with marine carbonate found in the Late Permian and Devono-Mississippian geologic record, respectively (Saltzman and Thomas, 2012). However, pristine limestone from the Late Permian Klondike assemblage and Devono-Mississippian Nasina assemblage would both be expected to have significantly heavier $\delta^{18}O_{VSMOW}$ signatures of ~+18 to +22‰ (Grossman, 2012). Rayleigh fractionation during open-system metamorphic degassing of CO_2 could produce a similar effect in $\delta^{18}O$. However, this effect would also shift $\delta^{13}C$ to lower values, which is not observed. The discrepancy may instead be explained by interaction with ^{18}O-depleted fluids during diagenesis. In addition, some degree of isotopic exchange with Yukon's modern ^{18}O-depleted meteoric water cannot be excluded ($\delta^{18}O_{VSMOW}$ ~-18 to -25‰; Bowen and Wilkinson, 2002).

   Relative to calcite marble of the Nasina assemblage, calcite in graphite-bearing schist of the Nasina assemblage is distinctly $\delta^{13}C$-depleted. The presence of tremolite in parts of the Nasina assemblage stratigraphy indicates CO_2 degassing via the reaction $5\ CaMg(CO_3)_2 + 8\ SiO_2 + 1\ H_2O = 1\ Ca_2Mg_5Si_8O_{22}$ (tremolite) $+ 3\ CaCO_3 + 7\ CO_2$. In open system degassing, fractionation of isotopically heavy CO_2 would drive the calcite reaction product to isotopically lower values of both $\delta^{13}C$ and $\delta^{18}O$. Alternatively, a depleted $\delta^{13}C$ signature may indicate the formation of calcite via the oxidation of isotopically light, organic-derived graphite.

2. C isotopes in the Klondike schist: Carbonate within the Klondike schist, regardless of paragenesis, shows a fairly narrow $\delta^{13}C_{VPDB}$ range of -13 to -2‰. This range of values is typical of carbonate in many orogenic gold camps worldwide (Nesbitt, 1991). The data also preclude any influence from externally-sourced sedimentary organic matter, *i.e.*, from the underlying Nasina assemblage, or from rare graphitic schist contained within the Klondike assemblage. The Klondike carbonate contrasts with other Phanerozoic examples of orogenic gold mineralization in which ^{13}C-depleted hydrothermal carbonate is sourced from reduced, biogenic sources of carbon in the wallrock (*e.g.*, gold deposits of Meguma terrane in Nova Scotia; Kontak and Kerrich, 1997).

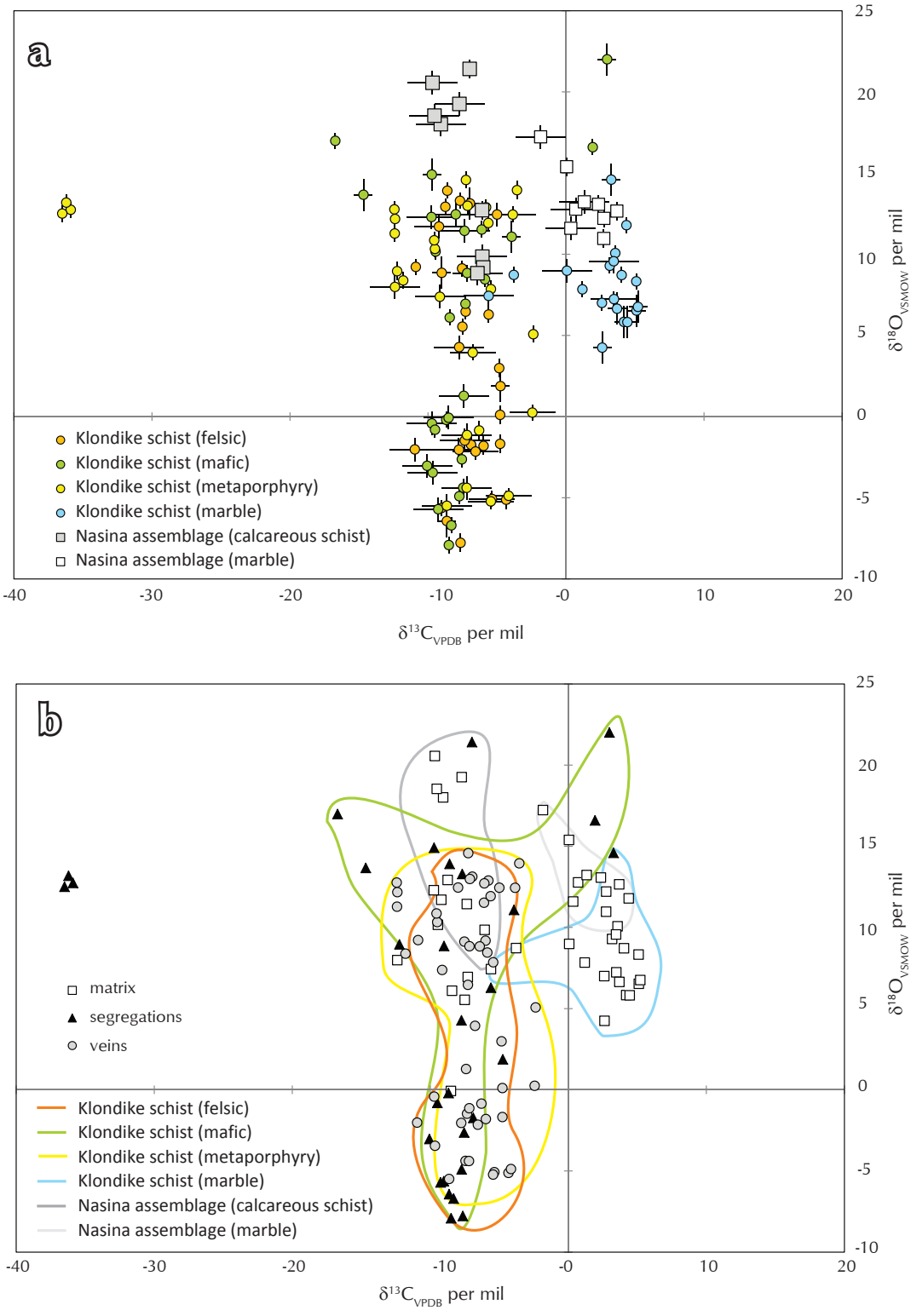

***Figure 7**. Carbon and oxygen isotopic ratios for Klondike carbonate samples; (a) plot of $\delta^{13}C_{VPDB}$ vs. $\delta^{18}O_{VSMOW}$, samples coloured by host rock lithology; and (b) sample plot as in (a), with data organized by mode of carbonate occurrence.*

3. O isotopes in the Klondike schist: The Klondike schist samples show a significant variation in $\delta^{18}O_{VSMOW}$, with no systematic difference between the different modes of carbonate occurrence. Some variation in oxygen isotopes is expected due to rock-fluid interaction during metamorphism, or by temperature-dependent fractionation of ^{18}O between minerals and CO_2 during hydrothermal activity. However, excursions to negative $\delta^{18}O_{VSMOW}$ values as low as -8‰ are not readily explained by these processes.

   Two main possibilities are considered. Rushton *et al.* (1993) collected δD data from fluid inclusions and hydrothermal minerals associated with gold-bearing veins in the Klondike, and argued that the 300 to 350°C fluids responsible for mineralization had a modified meteoric signature. However, the oxygen isotopic composition of hydrothermal carbonate is strongly rock-buffered, so a preserved meteoric signature is unlikely. The second possibility is interaction in the weathering environment with modern, ^{18}O-depleted meteoric water. Although care was taken to select only fresh, unaltered carbonate samples, relatively little exchange between calcite and meteoric water would be required to produce negative shifts in $\delta^{18}O_{VSMOW}$.

4. Origin of carbonate segregations: Textural observations indicate that segregations accumulate carbonate in the same manner as quartz, *i.e.*, migration by dynamic recrystallization during progressive deformation. Disseminated porphyroblasts of calcite, observed in some exposures of chloritic Klondike schist, are the most likely source of this remobilized carbonate. Both segregation carbonate and porphyroblastic ("matrix") carbonate yield $\delta^{13}C_{VPDB}$ values in the range from -15 to -3‰. These data are consistent with the preservation of C-isotopic signatures during ductile deformation, indicating closed-system behaviour (Appendix 2).

5. Origin of vein carbonate: The C and O isotopic signature of carbonate in D_4-stage veins maps remarkably well onto the signature of matrix and segregation carbonate in the Klondike schist host rocks. Although there are temperature and kinetic factors that can complicate interpretations of these signatures, these veins formed at mid-crustal levels in the absence of magmatism, and therefore, under pseudo-isothermal conditions. Rushton *et al.* (1993) concluded from fluid inclusion studies that most gold-stage veins in the Klondike formed at 300 to 350°C. Furthermore, vein carbonate in the Klondike shows no textural evidence for rapid precipitation, so hydrothermal conditions probably approximated isotopic equilibrium. Therefore, it is reasonable to suggest that the C isotopic signature of vein carbonate reflects the CO_2 from which it was derived. Although the range of measured $\delta^{13}C_{VPDB}$ values in vein carbonate from the Klondike (-12 to -2‰) are typical of volcanic-hosted orogenic gold deposits (Nesbitt, 1991), the data do not reveal an unambiguous source of CO_2. A number of sources could be considered, including: (1) metamorphic devolatization, especially of mafic rocks; (2) magmatic CO_2, either of crustal or mantle origin; or (3) CO_2 derived from a combination of ^{13}C-depleted and ^{13}C-enriched sources.

   A likely explanation for the source of carbonate in D_4-stage veins is that they derived their C isotopic signature from the local wallrock. This inference is supported by comparable $\delta^{13}C_{VPDB}$ values in veins and background (matrix or segregations) within the same sample (*e.g.*, see data for sample MA12-DL8 in Appendix 2). The strength of this relationship could be verified by targeting samples with a wider range of $\delta^{13}C_{VPDB}$ values, to test the hypothesis that carbon cycling between wallrock and hydrothermal fluids is a local phenomenon.

   The strong Nd-La correlation in Klondike schist carbonate may also support the notion that vein carbonate is locally derived. Figure 6 demonstrates that the Nd/La ratio in carbonate is consistent over orders of magnitude for matrix (porphyroblasts), segregations, and veins. This observation suggests that the system has been essentially closed with respect to rare earth elements since formation of the Klondike schist's volcanic protolith. Furthermore, absolute concentrations of Nd and La in carbonate from veins and segregations reach concentrations in the 10s of µg/g (ppm by weight), whereas concentrations in the matrix reach a maximum of a few µg/g. This may suggest that rare earth elements are progressively concentrated by carbonate remobilization into segregations, or by hydrothermal redistribution of carbonate into brittle structures.

CONCLUSIONS

Based on our field observations and preliminary isotopic evidence, we suggest the following sequence of events:

1. Carbonate was incorporated into the igneous protolith of the Klondike schist as alteration and/or veins during magmatic-hydrothermal activity in the Late Permian. During this time, small carbonate deposits formed at the seafloor, and later metamorphosed to form quartz-muscovite bearing marble.
2. Carbonate was segregated into quartz-rich layers during Late Permian D_1-D_2 deformation, during which it preserved its C-isotopic signatures.
3. Carbonate was re-concentrated into quartzose segregations during Early Jurassic D_3 deformation.
4. In the Late Jurassic, the onset of brittle D_4 deformation allowed aqueous hydrothermal solutions to leach carbonate stored by wallrock in segregations or in the rock matrix, to enter into fracture systems, and to precipitate quartz, carbonate, pyrite, and gold in veins.

The results of our study are consistent with $\delta^{13}C$ carbonate signatures being preserved in the Klondike schist during each of the above stages. Most importantly, carbonate in gold-bearing veins has a C-isotopic signature consistent with local host rock derivation of CO_2. Similarly, host rock derivation of gold and other vein components is a viable hypothesis.

This carbonate study is part of ongoing structural, geochemical, and geochronological studies of orogenic gold mineralization in Yukon. Further work on carbonate geochemistry should consider:

1. Integrating carbonate geochemistry with bulk rock compositional data;
2. Integrating carbonate geochemistry with stable (S, O, H) and radiogenic (Sr, Pb) isotopic studies of other minerals, to improve constraints on the source(s) of volatiles and metals;
3. Evaluating possible effects of surface weathering on stable isotopes.

ACKNOWLEDGEMENTS

This research was supported by MDRU's Yukon Gold Project – an industry-funded collaboration with sponsor companies Aldrin Resource Corp., Barrick Gold Corp., Full Metal Minerals Corp., Gold Fields Canada Exploration, Northern Freegold Resources Ltd., Kinross Gold Corp., Radius Gold Inc., Silver Quest Resources Ltd., Taku Gold Corp., Teck Resources Ltd., and Underworld Resources Inc. The Yukon Gold Project also benefitted from a NSERC Collaborative Research and Development grant. We thank Klondike Gold Corp. for allowing access to drill core and for providing collar coordinates, and Tim Liverton for providing additional samples.

We gratefully acknowledge Dr. Andreas Beinlich for guidance with stable isotope analysis, and Dr. Marg Amani for assistance with laser ablation ICP-MS measurements.

The manuscript benefited from a thoughtful review by Dave Craw from the University of Otago.

REFERENCES

Allan, M.M., Meier, D., and Guillong, M., 2010. SILLS: Signal Integration for Laboratory Laser Systems, v.1.1.0, Matlab program.

Allan, M.M., Mortensen, J.K., Hart, C.J.R., Bailey, L.A., Sánchez, M.G., Ciokiewicz, W., McKenzie, G.G., and Creaser, R.A., 2013. Magmatic and metallogenic framework of west-central Yukon and eastern Alaska. *In*: Tectonics, metallogeny, and discovery: the North American Cordillera and similar accretionary settings, M. Colpron, T. Bissig, B.G. Rusk, and J.F.H. Thompson (eds.), Society of Economic Geologists, Special Publication 17, p. 111-168.

Barker, S.L., Dipple, G.M., Dong, F., and Baer, D.S., 2011. Use of laser spectroscopy to measure the $^{13}C/^{12}C$ and $^{18}O/^{16}O$ compositions of carbonate minerals. Analytical Chemistry, vol. 83, no. 6, p. 2220-2226.

Beaudoin, G., 2011. The stable isotope geochemistry of orogenic gold deposits, *In:* 11th SGA Biennial Meeting, Antofagasta, Chile, 26-29 September, 2011. Society for Geology Applied to Mineral Deposits, Program with Abstracts, p. 556-558.

Beranek, L.P. and Mortensen, J.K., 2011. The timing and provenance record of the Late Permian Klondike orogeny in northwestern Canada and arc-continent collision along western North America. Tectonics, vol. 30, p. TC5017.

Bowen, G.J. and Wilkinson, B., 2002. Spatial distribution of $\delta^{18}O$ in meteoric precipitation. Geology, vol. 30, p. 315-318.

Breitsprecher, K. and Mortensen, J.K., 2004. Yukonage 2004: A database of isotopic age determinations for rock units from Yukon Territory. Yukon Geological Survey, CD-ROM.

Grossman, E.L., 2012. Oxygen isotope stratigraphy. *In*: The Geologic Time Scale 2012, F.M. Gradstein, J.G. Ogg, M. Schmitz, and G. Ogg (eds.), Elsevier, Boston, p. 181-206.

Groves, D.I., Goldfarb, R.J., Robert, F., and Hart, C.J.R., 2003. Gold deposits in metamorphic belts: Overview of current understanding, outstanding problems, future research, and exploration significance. Economic Geology, vol. 98, p. 1-29.

Hitzman, M., 1999. Routine staining of drill core to determine carbonate mineralogy and distinguish carbonate alteration textures. Mineralium Deposita, vol. 34, p. 794-798.

Hunt, P.A. and Roddick, J.C., 1992. A compilation of K-Ar ages: Report 21. Geological Survey of Canada Paper 91-2, p. 207-261.

Kontak, D.J. and Kerrich, R., 1997. An isotopic (C, O, Sr) study of vein gold deposits in the Meguma Terrane, Nova Scotia; implication for source reservoirs. Economic Geology, vol. 92, p. 161-180.

MacKenzie, D., Craw, D., and Mortensen, J.K., 2008a. Structural controls on orogenic gold mineralisation in the Klondike goldfield, Canada. Mineralium Deposita, vol. 43, p. 435-448.

MacKenzie, D., Craw, D., and Mortensen, J.K., 2008b. Thrust slices and associated deformation in the Klondike goldfields, Yukon. *In*: Yukon Exploration and Geology 2007, D.S. Emond, L.R. Blackburn, R.P. Hill, and L.H. Weston(eds.), Yukon Geological Survey, p. 199-213.

Mortensen, J., 1990. Geology and U-Pb geochronology of the Klondike District, west-central Yukon Territory. Canadian Journal of Earth Sciences, vol. 27, p. 903-914.

Mortensen, J.K., Dusel-Bacon, C., Hunt, J., and Gabites, J., 2006. Lead isotopic constraints on the metallogeny of middle and late Paleozoic syngenetic base-metal occurrences in the Yukon-Tanana and Slide Mountain/ Seventymile terranes and adjacent portions of the North American miogeocline. *In*: Paleozoic Evolution and Metallogeny of Pericratonic Terranes at the Ancient Pacific Margin of North America, Canadian and Alaskan Cordillera, M. Colpron, and J.J. Nelson(eds.), Geological Association of Canada Special Paper 45, p. 261-279.

Nesbitt, B., 1991. Phanerozoic gold deposits in tectonically active continental margins. *In*: Gold Metallogeny and Exploration, R.P. Foster(ed.), Blackie and Sons, Glasgow, p. 104-132.

Rushton, R.W., Nesbitt, B., Muehlenbachs, K., and Mortensen, J.K., 1993. A fluid inclusion and stable isotope study of Au quartz veins in the Klondike District, Yukon Territory, Canada; a section through a mesothermal vein system. Economic Geology, vol. 88, p. 647.

Saltzman, M.R., and Thomas, E., 2012. Carbon isotope stratigraphy. *In*: The Geologic Time Scale 2012, F.M. Gradstein, J.G. Ogg, M. Schmitz, and G. Ogg(eds.), Elsevier, Boston, 207-232.

Yukon MINFILE, 2010. Yukon MINFILE - A database of mineral occurrences. Yukon Geological Survey, <*http://data.geology.gov.yk.ca*> [accessed November 16, 2013].

APPENDIX 1. LA-ICP-MS data.

Sample	Carb. Type	Ca	Mg	Fe	Mn	Mineral	Zn	1σ	Sr	1σ	Y	1σ	Ba	1σ	La	1σ	Nd	1σ	Pb	1σ	U	1σ
		mol %	mol %	mol %	mol %		µg/g		µg/g		µg/g		µg/g		µg/g		µg/g		µg/g		µg/g	
K71	M	97.90	0.98	0.66	0.40	Mg-Fe-Mn cc	4.6	2.1	340	18	5	5	5.4	2.1	0.28	3.09	0.22	2.92	7.02	2.51	0.01	0.04
MA12-K03	M	99.73	0.02	0.06	0.15	cc	1.2	0.5	280	48	20	8	2.4	4.1	0.33	2.43	0.38	1.70	1.01	3.77	0.02	0.01
MA12-K07	M	97.97	1.04	0.66	0.26	Mg-Fe-Mn cc	4.6	3.1	276	202	15	8	13.1	22.4	0.39	9.14	0.29	7.00	9.65	5.35	0.05	0.02
MA12-K08	M	98.15	0.95	0.65	0.22	Mg-Fe-Mn cc	2.6	2.2	388	223	11	2	13.4	6.6	0.08	0.76	0.13	0.57	8.56	3.25	0.01	0.00
MA12-K09	M	97.58	1.18	0.85	0.36	Mg-Fe-Mn cc	3.3	1.3	515	434	13	6	15.4	5.4	0.49	2.31	1.23	2.93	16.97	7.82	0.06	2.20
MA12-K10	M	98.34	0.85	0.56	0.22	Mg-Fe-Mn cc	3.0	2.1	294	74	9	5	11.4	3.8	0.47	0.66	0.61	0.68	5.73	1.76	0.03	0.05
MA12-K12	M	98.42	0.78	0.54	0.22	Mg-Fe-Mn cc	3.4	1.8	428	116	14	6	7.3	5.4	0.05	1.25	0.09	0.75	6.27	2.43	0.01	0.01
MA12-K17	M	95.12	1.81	1.55	1.57	Mg-Fe-Mn cc	4.6	0.6	168	20	4	3	1.5	0.3	0.04	0.33	0.10	0.66	4.00	0.71	BD	
MA12-K20	M	95.39	1.81	1.53	1.22	Mg-Fe-Mn cc	2.5	0.6	187	328	7	4	12.2	2.8	0.06	0.59	0.28	0.80	4.10	7.28	0.01	0.00
MA12-K21	M	95.74	1.55	1.54	1.25	Mg-Fe-Mn cc	3.1	0.7	191	43	5	1	12.1	1.5	0.01	0.01	0.02	0.04	5.14	0.54	BD	
MA12-NAS6	M	96.17	3.27	0.22	0.06	Mg cc	4.1	3.0	2536	182	6	1	23.5	28.1	3.88	2.81	3.91	2.40	4.61	2.65	0.03	0.12
MA12-NAS9	M	96.45	2.56	0.77	0.12	Mg-Fe cc	15.8	3.2	362	14	7	1	5.2	0.9	0.02	0.32	0.23	0.34	1.88	0.11	0.01	0.00
MA12-NAS10	M	96.85	2.16	0.82	0.13	Mg-Fe cc	19.4	2.3	400	63	10	8	9.4	12.2	0.46	9.61	0.57	9.20	3.54	0.27	0.01	0.01
MA12-NAS11	M	99.02	0.44	0.35	0.07	cc	5.7	0.5	1021	37	6	1	4.5	0.7	2.08	0.25	1.69	0.19	7.83	1.06	BD	
MA12-NAS12	M	99.56	0.23	0.08	0.05	cc	4.2	0.3	706	38	4	0	33.4	2.5	1.88	0.11	1.08	0.09	1.39	0.15	0.01	0.03
05-LS-25_73.4m	S	54.77	39.68	4.47	0.85	Fe dol	230.8	37.1	371	66	8	17	5.6	2.2	8.49	22.46	8.08	18.25	12.48	3.29	0.14	0.03
MA12-DL1	S	97.02	0.99	0.59	1.08	Mg-Fe-Mn cc	1.5	4.8	235	216	29	8	16.1	18.9	2.42	1.22	6.17	1.93	21.07	2.33	0.11	0.10
MA12-DL3	S	93.45	2.75	2.02	1.61	Mg-Fe-Mn cc	4.4	1.1	800	61	29	6	6.1	8.9	0.03	0.02	0.07	0.08	40.48	4.89	0.26	0.78
MA12-DL6	S	96.71	1.46	0.66	1.01	Mg-Fe-Mn cc	2.0	2.0	1352	98	14	6	131.7	23.2	2.90	1.07	5.70	1.77	37.39	5.63	0.20	0.08
MA12-DL7	S	72.96	6.38	13.38	6.83	Fe-Mg-Mn cb			3808	1477	44	48	8000	10490	37.32	1.87	54.03	2.70	462	465	6.12	0.31
MA12-K05	S	98.95	0.35	0.26	0.38	Mg-Fe-Mn cc	5.1	0.6	537	36	72	3	16.3	1.1	0.07	0.09	0.30	0.07	21.35	2.30	BD	
MA12-K09	S	98.14	0.84	0.63	0.34	Mg-Fe-Mn cc	1.5	0.8	765	245	8	4	10.2	3.8	0.40	0.75	0.25	0.67	10.43	7.05	0.01	0.01
MA12-K14	S	51.62	41.20	6.57	0.44	Fe dol	130.3	51.9	314	140	33	6	6.0	3.6	2.49	0.69	3.84	1.00	22.20	47.51	0.07	0.15
MA12-K16	S	95.61	1.83	1.44	0.97	Mg-Fe-Mn cc	2.0	0.4	1281	33	9	0	6.1	1.0	0.01	0.00	0.05	0.01	37.32	4.80	BD	
MA12-NAS8	S	98.07	0.58	0.38	0.61	Mg-Fe-Mn cc	1.7	0.2	3045	165	48	5	17.9	1.0	0.20	0.03	1.21	0.13	5.72	0.36	0.01	0.02
MA12-SH1	S	94.45	2.95	0.82	1.64	Mg-Fe-Mn cc	21.9	9.7	1349	350	72	41	50.5	5.6	16.36	9.38	50.90	32.26	2.93	0.43	0.10	0.05
MA12-SH2	S	52.02	39.10	8.05	1.08	Fe dol	148.4	10.0	1103	80	11	4	88.0	9.7	2.35	0.99	4.46	2.11	6.19	2.12	0.02	0.02
BU-07-02_108.3m	V	96.20	2.28	0.75	0.59	Mg-Fe-Mn cc	8.4	24.7	1583	1651	15	17	14.2	5262.5	2.22	5.09	3.69	5.04	5.09	9.16	0.12	1.21
BU-07-02_114.6m	V	97.00	0.47	0.42	1.97	Mg-Fe-Mn cc			1152	504	168	38	20.1	39.2	65.06	59.74	54.78	23.82	0.16	0.04	0.01	0.00
BU-07-03_640m	V	95.88	1.17	0.97	1.76	Mg-Fe-Mn cc	1.0	0.4	1698	441	117	34	89.5	27.9	21.69	8.64	31.67	14.20	0.92	0.37	0.02	0.03
BU-07-03_78.6m	V	97.19	0.31	0.30	1.91	Mg-Fe-Mn cc	0.3	0.1	2165	668	21	14	72.8	33.1	2.92	1.98	3.38	3.53	0.14	0.05	0.07	0.04
BU-07-03_83.1m	V	97.45	0.30	0.30	1.81	Mg-Fe-Mn cc	0.3	0.0	1073	393	65	7	5.9	5.8	118.37	37.18	51.38	11.58	0.06	0.02	0.00	0.00
BU-07-03_91.7m	V	97.84	0.29	0.42	1.07	Mg-Fe-Mn cc			3345	575	44	4	88.6	27.9	13.12	2.14	13.28	1.09	0.19	0.06	0.02	0.00
BU-07-04_100.5m	V	97.13	0.57	0.78	1.09	Mg-Fe-Mn cc	0.4	0.2	3647	585	119	9	150.4	48.5	40.53	5.69	39.22	3.99	0.23	0.07	0.15	0.15
DDH-04-03_283.0m	V	95.16	1.64	1.20	1.67	Mg-Fe-Mn cc	0.8	0.1	2941	394	31	44	7.8	4.0	1.24	12.64	4.20	17.87	4.01	1.15	0.09	0.13
DDH-04-04_135.8m	V	98.42	0.19	0.29	0.85	Mg-Fe-Mn cc	0.6	0.5	666	350	97	42	12.3	4.8	72.17	53.07	61.58	28.47	3.09	28.77	0.04	0.15
DDH-04-04_87.0m	V	98.08	0.65	0.55	0.51	Mg-Fe-Mn cc	5.9	0.5	1800	253	28	4	27.2	4.4	0.32	1.29	0.52	1.18	45.31	5.48	0.16	0.13
DDH-04-05_149.3m	V	97.51	0.52	1.22	0.68	Mg-Fe-Mn cc	0.3		473	295	56	29	14.2	7.1	7.79	6.51	11.29	3.46	0.42	0.95	0.08	0.03
DDH-04-05_265.0m	V	98.86	0.11	0.13	0.85	Mg-Fe-Mn cc	0.4	0.2	357	167	218	95	2.0	1.6	49.11	31.22	62.89	32.38	0.27	0.13	0.01	0.03
DDH-04-05_314.5m	V	98.93	0.10	0.20	0.63	Mg-Fe-Mn cc			788	418	166	82	3.1	5.8	9.70	11.90	17.27	11.95	0.38	0.58	0.02	0.03
DDH-04-05_320.5m	V	70.85	20.41	8.08	0.50	Fe dol	188.2	52.4	648	717	69	60	25.0	69.5	35.64	40.34	31.39	40.39	20.61	12.98	0.19	0.14

APPENDIX 1. continued.

Sample	Carb. Type	Ca	Mg	Fe	Mn	Mineral	Zn	1σ	Sr	1σ	Y	1σ	Ba	1σ	La	1σ	Nd	1σ	Pb	1σ	U	1σ
		mol %	mol %	mol %	mol %		µg/g		µg/g		µg/g		µg/g		µg/g		µg/g		µg/g		µg/g	
DDH-04-05_322m	V	97.93	0.78	0.45	0.68	Mg-Fe-Mn cc	2.7	3.6	1765	531	16	10	16.0	6.8	2.72	3.37	2.63	3.42	17.03	3.44	0.10	0.13
DDH-04-05_332.4m	V	98.37	0.49	0.30	0.63	Mg-Fe-Mn cc	2.5	0.4	1713	481	8	3	33.0	6.2	0.02	0.03	0.04	0.05	40.14	9.87	BD	
DDH-04-05_333.6m	V	99.04	0.08	0.10	0.56	cc	0.5	0.1	2066	273	94	9	14.8	2.3	10.22	2.84	18.30	3.66	1.15	0.99	BD	
DDH-04-06_281.3m	V	97.75	0.41	0.82	0.65	Mg-Fe-Mn cc	2.7	15.3	3704	1474	20	43	15.5	8.9	1.59	1.77	1.60	2.67	18.13	6.71	0.42	0.35
MA12-DL5	V	98.27	0.62	0.43	0.58	Mg-Fe-Mn cc	0.8	0.3	864	62	10	2	6.0	0.8	0.04	0.04	0.07	0.07	26.71	2.00	0.01	0.01
MA12-DL6	V	96.51	1.73	0.61	0.90	Mg-Fe-Mn cc	3.4	4.2	1285	195	29	23	109.1	54.8	5.02	8.55	8.51	10.44	31.93	14.36	0.12	3.16
MA12-DL7	V	98.84	0.42	0.18	0.55	Mg-Fe-Mn cc	1.8	2.7	399	386	15	9	3.1	3.7	3.72	2.84	4.28	3.44	11.52	74.85	0.05	0.29
MA12-DL8	V	98.16	0.62	0.46	0.65	Mg-Fe-Mn cc	1.3	0.3	838	63	8	3	5.7	2.7	0.02	0.01	0.03	0.03	26.13	1.89	0.01	0.01
MA12-DL9	V	98.34	0.48	0.43	0.64	Mg-Fe-Mn cc	0.9	0.2	800	74	5	2	4.5	0.9	0.01	0.27	0.02	0.27	17.70	2.58	0.06	0.00
MA12-NAS6	V	99.56	0.19	0.13	0.05	cc	1.1	0.7	974	641	12	3	23.8	15.8	5.80	2.51	4.47	1.62	0.04	0.04	0.02	0.01
MA12-NAS6	V	98.32	0.17	1.23	0.17	Mg-Fe-Mn cc	109.6	52.5	240	126	22	18	17.1	9.8	6.91	9.54	6.55	10.71	0.76	0.90	0.32	0.14
MA12-SH3	V	96.81	0.86	0.47	1.06	Mg-Fe-Mn cc	0.5	1.0	1001	515	42	27	2.8	20.0	1.25	0.56	6.22	4.72	0.34	0.19	BD	
MA12-VG1	V	97.43	0.54	1.45	0.15	Mg-Fe-Mn cc	49.1	7.4	3984	724	52	9	2.3	1.4	4.05	0.73	9.18	0.87	610.10	155.86	8.61	1.12
MA12-VG2	V	97.34	0.04	1.15	0.46	Mg-Fe-Mn cc	3.2	0.2	8277	1173	522	146	29.2	8.6	2.22	0.69	7.51	2.65	62.98	11.37	0.01	0.00
MA12-VG3	V	96.40	0.50	1.31	0.68	Mg-Fe-Mn cc	4.7	1.4	9309	678	266	56	12.5	4.0	9.23	26.26	23.28	17.84	13.60	1.44	0.02	0.03
MA12-VG4	V	98.45	0.66	0.55	0.15	Mg-Fe-Mn cc	7.4	2.5	952	214	6	13	0.6	0.8	0.26	0.83	0.77	0.69	140.29	110.12	6.81	4.94
MA12-VG5	V	98.14	0.03	1.07	0.37	Mg-Fe-Mn cc	2.2	5.0	4072	250	143	52	8.5	3.7	0.62	3.36	3.86	3.80	71.91	20.03	0.01	1.15
MA12-VG6	V	96.20	0.35	2.45	0.19	Mg-Fe-Mn cc	3.3	0.4	6578	1085	247	88	10.6	5.3	8.56	2.85	26.04	7.97	52.32	20.17	0.05	0.09
MA12-VL5	V	96.90	0.56	0.81	1.04	Mg-Fe-Mn cc	4.4	1.2	5987	2689	31	10	149.0	91.2	2.08	5.70	4.31	5.39	61.04	13.38	0.02	0.00
MA12-VL6	V	98.69	0.22	0.39	0.07	Mg-Fe-Mn cc	3.4	0.5	5641	762	8	4	13.1	3.5	0.85	0.39	2.54	1.04	60.92	8.59	BD	
MA12-VL7	V	97.50	0.38	0.47	0.83	Mg-Fe-Mn cc	3.6	1.8	7134	924	78	29	119.4	207.4	5.43	11.23	14.68	12.87	64.42	18.67	0.02	0.27
MA12-VL8	V	98.35	0.41	0.62	0.53	Mg-Fe-Mn cc	4.4	0.5	791	128	28	3	30.5	6.8	0.53	0.77	1.09	0.80	98.23	13.93	0.01	0.01

NOTES

cc = calcite; dol = dolomite; cb = generic carbonate

BD = below detection

APPENDIX 2. CO isotopes.

Sample	Carb. Type	$\delta^{13}C_{VPDB}$ (per mil)	1σ	$\delta^{18}O_{VSMOW}$ (per mil)	1σ
Klondike schist (felsic)					
05-LS-25_75.0m	S	-6.88	0.23	-1.73	0.57
	S	-7.64	0.23	-7.77	0.57
BU-07-02_114.6m	V	-4.34	0.23	-5.12	0.57
BU-07-02_146.2m	V	-10.95	1.80	-2.02	0.72
BU-07-03_64.0m	V	-4.78	0.23	0.11	0.57
BU-07-03_78.6m	V	-4.78	0.23	-1.67	0.57
BU07-03_91.7m	V	-5.98	0.23	-1.80	0.57
BU-07-04_100.5m	V	-4.84	0.23	2.99	0.57
DDH-04-03_283.0m	V	-7.76	1.80	-2.04	0.72
DDH-04-03_322m	V	-6.55	1.64	-2.15	0.48
DDH-04-04_106.5m	V	-7.34	1.80	-1.47	0.72
DDH-04-04_108.5m	V	-5.00	1.80	12.45	0.72
DDH-04-04_135.8m	V	-5.36	1.64	-5.07	0.48
MA12-DL1	S	-4.75	0.66	1.88	0.99
	S	-5.61	0.26	6.29	0.49
	S	-7.74	1.80	4.28	0.72
MA12-DL2	S	-7.69	0.26	13.29	0.49
MA12-DL3	S	-8.60	0.26	13.92	0.49
	S	-9.01	0.66	8.86	0.99
MA12-DL4	S	-8.64	0.66	-6.43	0.99
	S	-9.02	0.26	-5.63	0.49
MA12-DL5	V	-6.96	0.66	13.13	0.99
MA12-K19	V	-10.89	0.26	9.22	0.49
MA12-K20	M	-7.51	0.26	5.54	0.49
	M	-9.21	1.80	11.71	0.72
	V	-7.28	0.26	6.47	0.49
MA12-K21	M	-8.75	0.26	12.93	0.49
	V	-7.53	0.26	9.13	0.49

M = Matrix

S = Segregation

V = Vein

Sample	Carb. Type	$\delta^{13}C_{VPDB}$ (per mil)	1σ	$\delta^{18}O_{VSMOW}$ (per mil)	1σ
Klondike schist (metaporphyry)					
06-NZ-01_65.7m	M	-12.39	1.80	7.99	0.72
06-NZ-01_65.8m	S	-12.24	0.23	8.96	0.57
BU-07-03_83.1m	V	-6.30	0.23	-0.85	0.57
DDH-04-04-87.0m	V	-3.55	0.23	13.95	0.57
DDH-04-05_149.3m	V	-8.64	1.80	-5.49	0.72
DDH-04-05_314.5m	V	-5.45	1.64	-5.22	0.48
	V	-7.20	1.80	-4.39	0.72
DDH-04-05_320.5m	V	-6.76	1.64	3.95	0.48
DDH-04-05_332.4m	V	-3.86	1.64	12.45	0.48
DDH-04-05_333.6m	V	-4.16	1.64	-4.88	0.48
	V	-7.18	1.80	-1.13	0.72
DDH-04-06_281.3m	V	-9.14	1.80	7.38	0.72
DDH-04-06_32.0m	V	-2.44	1.64	0.25	0.48
MA12-VG1	V	-2.38	0.17	5.07	0.51
MA12-VG2	V	-5.63	0.17	11.93	0.51
MA12-VG3	V	-5.80	0.26	12.89	0.49
MA12-VG4	V	-5.45	0.17	7.85	0.51
MA12-VG5	V	-7.25	0.17	14.58	0.51
MA12-VG6	V	-7.13	0.17	12.99	0.51
MA12-VL5	V	-11.80	0.17	8.39	0.51
	V	-12.44	0.26	12.77	0.49
MA12-VL6	S	-35.88	0.26	12.74	0.49
	S	-36.21	0.26	13.19	0.49
	S	-36.50	0.17	12.51	0.51
MA12-VL7	V	-12.39	0.17	12.18	0.51
	V	-12.41	0.26	11.28	0.49
MA12-VL8	V	-9.50	0.26	10.33	0.49
	V	-9.55	0.17	10.87	0.51

M = Matrix

S = Segregation

V = Vein

APPENDIX 2. continued.

Sample	Carb. Type	$\delta^{13}C_{VPDB}$ (per mil)	1σ	$\delta^{18}O_{VSMOW}$ (per mil)	1σ
Klondike schist (mafic)					
BU-07-02_108.3m	V	-7.41	1.80	1.28	0.72
MA12-DL6	M	-7.29	0.26	6.95	0.49
	S	-7.73	0.26	-4.90	0.49
	V	-9.66	1.80	-3.45	0.72
	V	-9.72	1.80	-0.42	0.72
MA12-DL7	S	-9.73	0.66	14.91	0.99
	V	-7.16	0.17	8.84	0.51
MA12-DL8	M	-7.36	1.80	11.45	0.72
	M	-8.43	0.26	6.11	0.49
	V	-7.99	1.80	12.46	0.72
MA12-DL9	V	-5.87	0.26	8.46	0.49
	V	-6.11	0.17	11.53	0.51
MA12-K05	S	-14.68	0.66	13.67	0.99
	S	-16.72	0.26	16.99	0.49
MA12-K14	S	2.97	0.66	22.01	0.99
	S	1.93	0.26	16.60	0.49
MA12-K16	S	-3.94	0.66	11.09	0.99
MA12-K17	M	-9.45	0.26	10.17	0.49
	M	-9.75	1.80	12.30	0.72
MA12-SH1	S	-7.55	0.17	-2.63	0.51
	S	-8.31	0.26	-6.70	0.49
	S	-8.68	0.26	-0.20	0.49
	S	-9.26	1.80	-5.71	0.72
MA12-SH2	S	-8.49	0.17	-7.91	0.51
	S	-9.49	0.26	-0.80	0.49
	S	-10.06	1.80	-3.03	0.72
MA12-SH3	M	-8.51	1.80	-0.07	0.72
	V	-7.45	0.23	-4.38	0.57
Klondike schist (marble)					
K70	M	0.06	1.80	8.99	0.72
K71	M	3.47	1.64	7.24	0.48
K72	M	-3.79	0.26	8.73	0.49
	M	-5.61	1.80	7.44	0.72
MA12-K07	M	5.10	0.66	6.53	0.99
	M	4.19	0.66	5.84	0.99
	M	4.03	0.26	8.72	0.49
	M	3.57	0.26	10.08	0.49
MA12-K08	M	3.70	0.66	6.65	0.99
	M	3.17	0.26	9.29	0.49
MA12-K09	M	2.61	0.66	4.25	0.99
	M	1.19	0.26	7.84	0.49
	S	3.27	0.66	14.60	0.99
MA12-K10	M	5.21	0.66	6.76	0.99
	M	4.37	0.26	11.79	0.49
	M	3.45	1.80	9.57	0.72
MA12-K11	M	2.60	0.26	7.00	0.49
MA12-K12	M	5.08	0.26	8.33	0.49
	M	4.44	0.66	5.82	0.99

M = Matrix

S = Segregation

V = Vein

APPENDIX 2. continued.

Sample	Carb. Type	$\delta^{13}C_{VPDB}$ (per mil)	1σ	$\delta^{18}O_{VSMOW}$ (per mil)	1σ
Nasina assemblage (calcareous schist)					
MA12-NAS5	M	-7.73	1.80	19.26	0.72
MA12-NAS6	M	-6.06	1.80	9.85	0.72
	V	-6.00	0.23	9.19	0.57
	V	-6.09	0.23	12.72	0.57
	V	-6.42	1.80	8.84	0.72
MA12-NAS7	M	-9.07	1.80	18.01	0.72
	M	-9.53	1.80	18.54	0.72
	M	-9.68	1.80	20.57	0.72
MA12-NAS8	S	-6.98	0.23	21.42	0.57
Nasina assemblage (marble)					
MA12-NAS9	M	3.68	0.23	12.66	0.57
	M	0.71	1.80	12.78	0.72
MA12-NAS10	M	2.74	0.23	12.21	0.57
	M	2.73	0.23	10.97	0.57
	M	1.32	1.80	13.23	0.72
	M	0.35	1.80	11.60	0.72
MA12-NAS11	M	2.35	0.23	13.08	0.57
MA12-NAS12	M	0.04	0.23	15.39	0.57
	M	-1.84	1.80	17.23	0.72

M = Matrix

S = Segregation

V = Vein